Structural and mechanical properties of a polyethylene-based thermoplastic elastomer

Roland Séguéla
Laboratoire de Structure et Propriétés de l'Etat Solide, UA CNRS 234, Université de Lille I, 59655 Villeneuve d'Ascq Cédex, France

and Jacques Prud'homme
Department of Chemistry, University of Montreal, Montreal (Quebec), H3C 3V1 Canada
(Received 11 July 1988; revised 21 November 1988; accepted 18 January 1989)

The thermal behaviour, mesomorphic structure and thermomechanical properties of a hydrogenated poly(butadiene-*b*-isoprene-*b*-butadiene) triblock polymer have been investigated in relation to the morphogenesis conditions. The material was cast into films crystallized from the melt or from a benzene solution. The first method involves intermolecular crystallization of the hydrogenated polybutadiene blocks within microdomains owing to the phase separation of the unlike species in the melt, which is discussed on experimental grounds and thermodynamic considerations. This process imparts good elastomeric properties to the melt-crystallized material. The second method proceeds from a dilute homogeneous medium, which promotes intramolecular crystallization of the hydrogenated polybutadiene blocks and prohibits physical crosslinking of the chains. The solution-crystallized material exhibits a strong creep effect under low stress. The study of the structural changes on drawing by means of small angle and wide angle X-ray scattering corroborates the conclusions inferred from the mechanical behaviour.

(Keywords: semi-crystalline block polymer; hydrogenated polybutadiene; hydrogenated polyisoprene; mechanical properties; mesomorphic structure; thermal behaviour)

INTRODUCTION

Elastomeric ABA triblock polymers with rubbery midblock and glassy endblocks are well known to exhibit unique structural and mechanical properties owing to the phase separation of the unlike moieties on a molecular scale which involves a physical crosslinking of the chains[1–3]. Since the early sixties, considerable attention has been paid to poly(styrene-*b*-diene-*b*-styrene) thermoplastic elastomers, which are commercially available in wide ranges of compositions and molecular weights. More recently, investigations have been oriented towards the improvement of dimensional stability at high temperature. In this connection, AB and ABA block polymers having semi-crystalline A blocks with high melting temperature such as polydiphenylsiloxane[4], poly(ethylene sulphide)[5,6], polypivalolactone[7,8] and polycaprolactam[9] have been synthesized and studied. It is worth mentioning that block polymers having low melting temperature blocks have also aroused deep interest as model systems, for theoretical investigations[2,3,5,10–14].

Semi-crystalline ABA triblock polymers consisting of hydrogenated polydiene blocks deserve particular attention since they are related to polyolefin-based thermoplastic elastomers, usually obtained via Ziegler–Natta copolymerization of olefins[15]. Indeed, hydrogenation of polybutadiene with predominant 1,4 microstructure leads to a crystallizable polyethylene-like chain containing a few randomly distributed 1-butene units due to the former 1,2 microstructure units[16,17]. In contrast, hydrogenated polybutadiene with high 1,2 microstructure level and hydrogenated polyisoprene are amorphous polymers with rubbery properties at room temperature[16,18]. One of the main reasons for preparing hydrogenated polydiene block polymers from anionically polymerized substrates lies in the well defined structure and architecture together with the low molecular weight polydispersity of such materials compared with Ziegler–Natta products. This allows more systematic investigations of structure–property relationships as well as comparisons with parent homopolymers having similar molecular characteristics to the various blocks.

Falk and Schlott[16] reported good tensile strength and elongation at break data for fully hydrogenated triblock polymers of butadiene based on 1,4 microstructure-rich endblocks and 1,2 microstructure-rich midblocks, for a wide range of compositions. These authors also investigated a series of triblock polymers having polyisoprene midblocks and selectively hydrogenated polybutadiene endblocks of high 1,4 microstructure level[19]. Following these works, Mohajer *et al.*[20,21] studied morphological, thermal and mechanical properties of fully hydrogenated (H) diblock and triblock polymers of butadiene (B) and isoprene (I) as a function of composition and sequence architecture. It has been shown that HBI diblock polymer as well as HBIB and HIBI triblock polymers exhibits good phase separation in the solid state. However, HBI and HIBI polymers show very much higher energy loss than HBIB polymers during cyclic deformation as a result of their inability to form permanent physical crosslinks.

The present work is concerned with the influence of morphogenesis (i.e. the process of formation of the mesomorphic structure) on thermal, structural

0032-3861/89/081446-10$03.00

and mechanical properties of a fully hydrogenated poly(butadiene-*b*-isoprene-*b*-butadiene) triblock polymer. The polybutadiene hydrogenated weight fraction, $W_{HB} \approx 0.27$, has been chosen to give rise to a continuous polyisoprene hydrogenated phase with an overall elastomeric behaviour of the material. We have focused our attention on samples prepared by crystallization from the melt or from solution. The first method relies on a bulk state crystallization of the polybutadiene hydrogenated blocks within more or less dispersed domains. This assumes a liquid–liquid phase separation of the unlike moieties in the melt, which will be discussed. In the second method, crystallization proceeds from a homogeneous and dilute state.

EXPERIMENTAL

Synthesis and molecular characterization

The poly(butadiene-*b*-isoprene-*b*-butadiene) triblock polymer, BIB, was anionically prepared by sequential polymerization of butadiene and isoprene in benzene at room temperature, according to standard techniques[22]. The initiator was *sec*-butyllithium at a concentration of $\approx 4 \times 10^{-4}$ M and the termination agent was *tert*-butanol. Catalytic hydrogenation was carried out in cyclohexane at 323 K, under 1 MPa hydrogen pressure, following a method previously described[18]. The Ziegler-type catalyst was prepared from triethylaluminium and cobalt(II) octoate, with a molar ratio Al/Co = 3. The cobalt to unsaturation ratio was close to 0.2. After the hydrogenation was complete, water was added to the reaction medium to stop the catalyst activity and to help extract the catalytic residues from the organic solution. Simultaneous addition of hexamethylphosphoramide improved flocculation and separation of the residues[23]. The organic solution was then filtered and the polymer precipitated into methanol. The hydrogenated triblock polymer is denoted HBIB.

Parent hydrogenated polybutadiene (HPB) and hydrogenated polyisoprene (HPI) homopolymers were prepared according to the same procedure.

Composition and microstructures were determined from 220 MHz nuclear magnetic resonance (n.m.r.) spectra of the polymers, before hydrogenation. The disappearance of any *unsaturated* resonance on the spectra of the hydrogenated products was taken as an evidence of the hydrogenation efficiency. Number-average molecular weights were determined from osmotic pressure measurements in toluene, using an automatic Hewlett–Packard apparatus provided with a Schleicher–Schuell cellulosic membrane. Analyses of the triblock polymer by gel permeation chromatography (g.p.c.) were performed on Waters Associates GPC 200 equipment, with tetrahydrofuran as solvent.

Sample preparation

Two kinds of films of the HBIB hydrogenated triblock polymer were prepared by two different methods. The first method involved slow evaporation of the solvent from a 3% xylene solution at 365 ± 2 K for 3 d. The molten polymer was then isothermally crystallized for 3 d at 345 ± 2 K, i.e. in the range of maximum crystallization rate, before cooling at 5 K min^{-1}. This method was expected to impart a stable morphology owing to the solidification of the block polymer from a thermodynamically stable melt, after phase separation of the unlike moieties. The second method was based on the crystallization of a 1% benzene solution by slow cooling from 335 K down to room temperature, before evaporating the solvent. In this case, the final morphology was obviously metastable since crystallization occurred in a dilute medium, before phase separation.

Xylene and benzene were chosen for their good solvent quality with regard to the two block species in order not to affect the morphology of the solid materials. Benzene was preferred in the second method because of better evaporation capability at room temperature. In both cases, the solution was poured over a mercury surface, within a stainless steel frame. Evaporation was conducted under controlled pressure. The solid films were finally stored under vacuum for a week at least, at room temperature. Their thickness was in the range 0.2–1 mm.

Physical characterization

Calorimetric investigations were carried out on a Perkin–Elmer DSC-2 apparatus, the samples having a mass close to 15 mg. The temperature scale and melting peak areas were calibrated by running samples of mercury ($T_f = 234$ K, $\Delta H_f = 2.7$ cal g^{-1}) and indium ($T_f = 430$ K, $\Delta H_f = 6.8$ cal g^{-1}). The weight crystallinity, X_c^w, was calculated from the relation

$$X_c^w = \Delta H_f / \Delta H_f^* \quad (1)$$

where ΔH_f is the enthalpy of fusion of the polymer per gram of crystallizable species, and $\Delta H_f^* = 69$ cal g^{-1} is that of an infinite perfect crystal of polyethylene at $T_f = 413$ K (Reference 24).

Density determinations were performed at 296 K in a water–isopropanol gradient column calibrated by means of seven glass beads of known density in the range 0.82–0.94 g cm^{-3}. The weight crystallinity was estimated from the equation

$$X_c^w = (\rho_c/\rho)(\rho - \rho_a)/(\rho_c - \rho_a) \quad (2)$$

which assumes a perfect two-phase model, where ρ is the density of the polymer, and $\rho_a = 0.855$ g cm^{-3} and $\rho_c = 1.000$ g cm^{-3} are the amorphous and crystalline densities, respectively[24].

The small angle X-ray scattering (SAXS) study was carried out on a Model 2202 Rigaku-Denki goniometer equipped with two pinhole collimators of 0.5 and 0.3 mm diameter. The second pinhole, sample and photographic film were placed at 300, 320 and 630 mm from the first pinhole, respectively. The nickel-filtered CuKα radiation ($\lambda = 0.154$ nm) was generated by a Philips tube operated at 40 kV and 20 mA. The sample strain in the region of the SAXS analysis was determined from the displacement of ink marks, 1 mm apart before deformation. The sample thickness was in the range 0.5–1 mm. The photographic films were optically scanned on a Joyce–Loebl recording microdensitometer.

Wide angle X-ray scattering (WAXS) diagrams were recorded on a flat-film Statton–Warhus camera fitted with two pinhole collimators of 0.7 and 0.5 mm diameter. The second collimator close to the sample and the film were placed at 50 and 100 mm, respectively, from the first pinhole.

Mechanical measurements

Stress–strain curves were recorded using an Instron tensile testing machine. The test pieces were in the form of strips 50 mm long and 5 mm wide. The sample thickness was in the range 0.2–0.4 mm. The crosshead speed was 40 mm min^{-1} and the samples were allowed to relax unloaded for 10 min between two consecutive deformation cycles. The draw ratio is defined as $\alpha = L/L_0$.

Dynamic mechanical experiments were conducted on a Toyo–Baldwin viscoelastometer Rheovibron Model DDV-II B. The test pieces were 10–20 mm long, 5 mm wide and 0.4–1 mm thick. Measurements were made as a function of temperature at average intervals of 3 K. The data were corrected for apparatus compliance and sample shearing in the grips by using an empirical correction factor determined at near zero sample length as a function of temperature, as suggested by the apparatus manufacturer.

RESULTS AND DISCUSSION

Materials

According to the n.m.r. analysis, the homopolybutadiene and polybutadiene blocks in the triblock polymer have a microstructure composed of 90% 1,4-(*cis* + *trans*) units and 10% 1,2 units, while the microstructure of the homopolyisoprene and polyisoprene blocks in the triblock polymer is composed of 71% 1,4-*cis* units, 22% 1,4-*trans* units and 7% 3,4 units. The number average molecular weight of the block polymer is $\overline{M}_n = 157 \times 10^3$ and its polybutadiene weight fraction $W_{PB} = 0.27$. The polybutadiene and polyisoprene homopolymers have number average molecular weights $\overline{M}_n = 56 \times 10^3$ and 57×10^3, respectively.

The hydrogenated polybutadiene blocks (HB) in the hydrogenated triblock polymer (HBIB) and parent hydrogenated homopolybutadiene (HPB) are similar to ethylene/1-butene random copolymers containing 6 mol% 1-butene units, with good crystallization capabilities. On the other hand, the hydrogenated polyisoprene blocks (HI) in the hydrogenated triblock polymer and parent hydrogenated homopolyisoprene* (HPI) can be considered as alternating ethylene/propylene copolymers containing 3 mol% 3-methyl-1-butene units, with rubbery properties at room temperature.

Figure 1 shows the g.p.c. elution curves of the triblock polymer before (*Figure 1a*) and after (*Figure 1b*) hydrogenation, compared with a polystyrene standard. It appears from this figure that hydrogenation does not introduce significant chain degradation and that the HBIB polymer has unimodal molecular weight distribution and low polydispersity.

Thermal behaviour

Differential scanning calorimetry (d.s.c.) curves of the HBIB block polymer crystallized from the melt and solution are shown in *Figure 2*, together with the d.s.c. curves of the HPI and PHB parent homopolymers. The glass transition of the HI blocks (*Figure 2a, b* and *c*) occurs at the same temperature as for the HPI homopolymer (*Figure 2d*), whatever the thermal treatment of the block polymer. Moreover, the specific heat capacity jump at the glass transition of the HI blocks is equal to that of HPI homopolymer, within the limits of experimental accuracy. These features strongly argue for a good phase separation of the unlike species in the block polymer.

The situation is, however, less clear when analysing the thermal behaviour of the HB blocks. It can be seen from *Figure 2* that the shape of the melting peak as well as the maximum melting temperature (T_f^{max}) are different for the HB block and HPB homopolymer, for the same crystallization conditions (compare *Figure 2b* with *2e* and *Figure 2c* with *2f*). The broadening of the melting peak and lowering of the T_f^{max} of the HB blocks with regard to the HPB homopolymer indicate a broader distribution of thinner crystalline lamellae, which suggests a modification of the crystallization kinetics. On the other hand, crystallinity data from d.s.c. and density measurements reveal quite surprising properties, as shown in *Table 1*. Indeed, although the density data systematically surpass the d.s.c. ones because of different assumptions and approximations in the calculations, comparisons between data from the same method show that the HB block crystallinity is very close to that of the HPB homopolymer when crystallized from the melt. This is in agreement with the data of Mohajer *et al.*[20,21], which emphasize that the HB block crystallinity is independent of block polymer composition and architecture. When it deals with crystallization from solution,

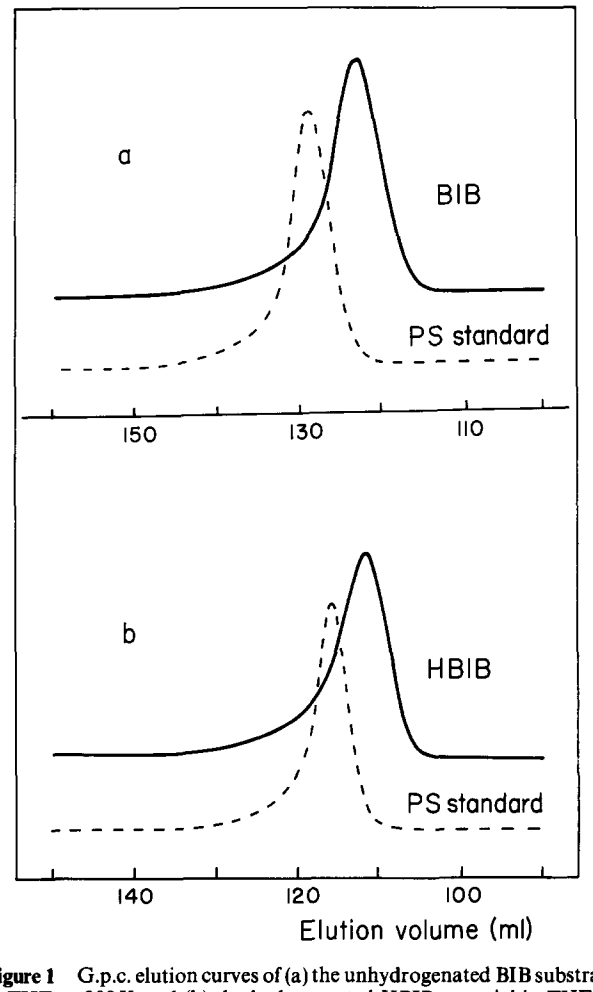

Figure 1 G.p.c. elution curves of (a) the unhydrogenated BIB substrate in THF at 308 K and (b) the hydrogenated HBIB material in THF at 323 K (PS standard: $M_n = 1.0 \times 10^5$, $M_w/M_n = 1.02$)

*HPI hydrogenated homopolyisoprene is referred as hydrogenated PI-8 in Reference 18.

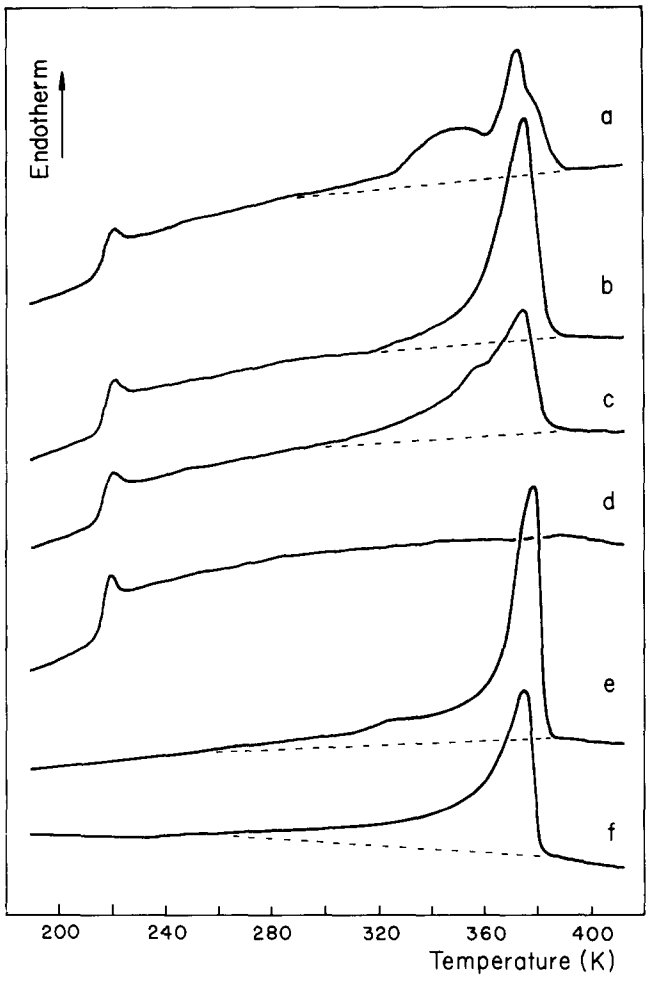

Figure 2 D.s.c. heating curves of (a) isothermally crystallized HBIB, (b) solution crystallized HBIB, (c) melt-crystallized HBIB by slow cooling at $-5\,K\,min^{-1}$, (d) amorphous HPI, (e) solution-crystallized HPB and (f) melt-crystallized HPB by slow cooling at $-5\,K\,min^{-1}$. The heating rate is $40\,K\,min^{-1}$

Table 1 Crystal weight fraction, X_c^w, at room temperature of the HB blocks in the HBIB triblock polymer and HPB homopolymer crystallized from the melt and from solution

	HBIB		HPB	
	M.c.[a]	S.c.[b]	M.c.	S.c.
X_c^w from d.s.c.	0.38	0.45	0.37	0.49
X_c^w from density	0.45	0.52	0.45	0.59

[a] M.c., melt crystallized
[b] S.c., solution crystallized

crystallinity is notably improved with regard to melt crystallization thanks to chain reeling[25]. However, in the case of the HBIB polymer, the HB block must drag the uncrystallizable HI block through the homogeneous solution so that their crystallization cannot be as easy as for the HPB homopolymer.

It is worth noting that the melting curve of the HB blocks in the HBIB block polymer isothermally crystallized from the melt (*Figure 2a*) reveals two crystallite distributions due, on the one hand, to the isothermal crystallization and, on the other hand, to the subsequent cooling.

Figure 3 shows the d.s.c. cooling curves of HBIB and HPB samples recorded at a $5\,K\,min^{-1}$ cooling rate.

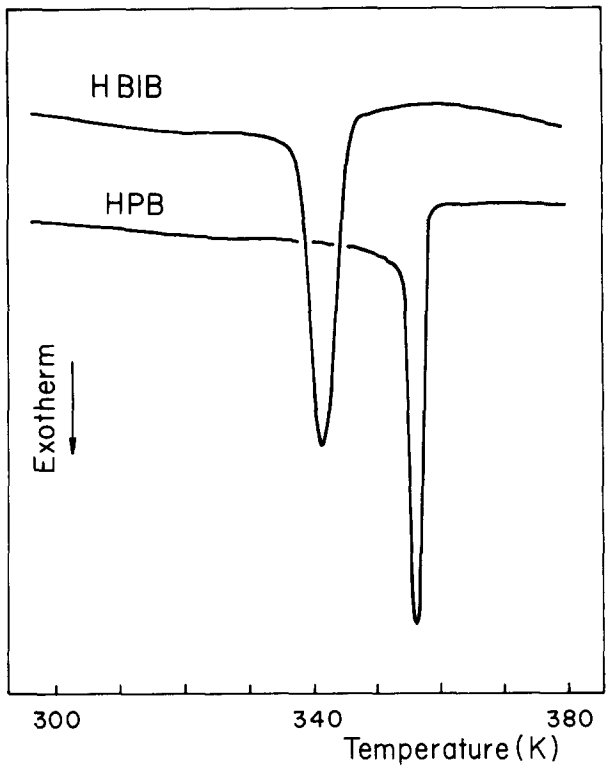

Figure 3 D.s.c. cooling curves of HBIB and HPB samples at cooling rate $-5\,K\,min^{-1}$

Crystallization onset of the HBIB polymer occurs about 14 K below that of the HPB homopolymers. Moreover, the width of the exothermic crystallization peak for the triblock polymer is twice that for the homopolymer. This gives additional evidence of a hindrance to the crystallization of the HB block, in agreement with the results of Mohajer *et al.*[20,21]. These authors suspected that an eventual mixing between the HI and HB blocks in the melt could be responsible for the crystallization retardation[20]. This suggestion was based on the fact that the non-hydrogenated block polymers display miscibility of the I and B blocks on a molecular scale[20]. We would like to emphasize, however, that from a thermodynamic standpoint, HI and HB blocks are in fact less compatible than I and B blocks. Indeed, the mixing capability of two polymers can be judged from the value of the square difference between their solubility parameters, δ. Using the Small attraction constants for the estimation of the solubility parameters[26], we obtain:

$$(\delta_I - \delta_B)^2 = 2 \times 10^{-3}\ \text{cal*}\ \text{cm}^{-3}$$

and

$$(\delta_{HI} - \delta_{HB})^2 = 8 \times 10^{-2}\ \text{cal}\ \text{cm}^{-3}$$

which indicate much poorer compatibility between HI and HB blocks than between I and B blocks.

In another context, Lindsay *et al.*[27] reported a study of blends of a polyethylene (PE) with ethylene/propylene rubbers (EPR) which deserves particular attention. This work shows that in a blend with a wholly amorphous EPR, the PE undergoes a 6 K depression of the crystallization onset, accompanied by a slight enlargement of the crystallization peak. The authors suggested that the solubility of ethylene sequences of the amorphous EPR within the molten PE was responsible for the

*1 cal ≈ 4.18 J

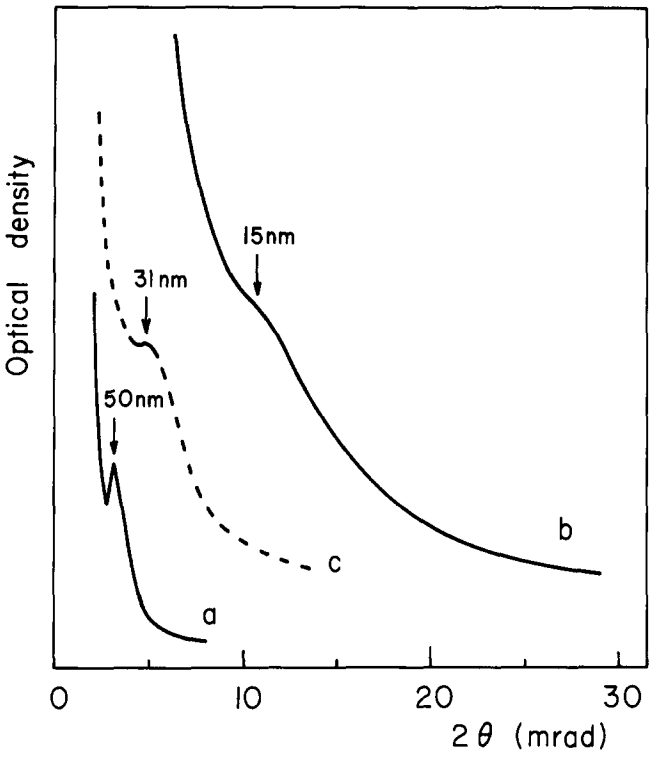

Figure 4 Microdensitometric traces of SAXS patterns from undeformed HBIB: (a) 12 h exposure and (b) 72 h exposure for a melt-crystallized sample; (c) 24 h exposure for a solution-crystallized sample

crystallization delay. In the present case, the amorphous HI blocks are similar to an alternating ethylene/propylene copolymer which only contains isolated ethylene units, so that the HB and HI blocks in the triblock polymer are less compatible than the PE and EPR in the blend mentioned above. Accordingly, compatibility cannot be invoked to account for the hindrance to the HB block crystallization.

It has been pointed out, in the case of phase-separated amorphous block polymers[28], that the glass transition temperature shift of the unlike species can be ascribed to a reciprocal interaction through the link between the unlike moieties in every chain. By analogy, it is likely that the interaction of the very soft and non-crystallizable HI blocks in the HBIB polymer could disturb the nucleation and growth of crystals of the HB blocks.

Mesomorphic structure

The mesomorphic structure of undeformed melt-crystallized and solution-crystallized samples of the HBIB block polymer was investigated by means of small angle X-ray scattering. Microdensitometric traces of the patterns are given in *Figure 4*.

The bulk-crystallized sample gives rise to a sharp reflection (*Figure 4a*) with a long period $L \approx 50$ nm characteristic of a regular packing of HB microdomains in the HI matrix, owing to the phase separation before crystallization. The diffuse reflection (*Figure 4b*) arises from the intercrystallite diffraction within the HB microdomains. The average distance between crystallites can be estimated to $l \approx 15$ nm. It has been reported by Kuo and McIntyre[13], for a melt-crystallized TCB–I–TCB three block polymer (TCB = polythiacyclobutane, I = polyisoprene) having a volume fraction $\phi_{TCB} \simeq 0.3$ of semi-crystalline TCB phase, that the TCB microdomains adopt a cylindrical structure and pack themselves in a two-dimensional hexagonal array. It is worth mentioning that this is the basic mesomorphic structure of AB and ABA amorphous block polymers with $0.15 < \phi_A < 0.35$[1], but the lack of higher orders did not allow confirmation in the present case. So, assuming that this structure also prevails in the melt-crystallized HBIB, given its HB volume fraction $\phi_{HB} \approx 0.25$, one can assess the HB cylinder radius to be $R \approx 16$ nm using the relation[3]

$$R = (3^{\frac{1}{2}}\phi_{HB}/2\pi)^{\frac{1}{2}}a \quad (3)$$

In this relation, the unit cell parameter a is given by

$$a = 2L/3^{\frac{1}{2}} \quad (4)$$

since the long period L is that of the first (10) reflection of the two-dimensional hexagonal lattice.

Comparison of the HB cylinder radius, $R \approx 16$ nm, with the intercrystallite distance, $l \approx 15$ nm, shows that no more than two crystallites can be accommodated within the microdomain cross section. This may be a reason for the very diffuse intercrystallite diffraction.

For the solution-crystallized sample, a single broad reflection is observed in *Figure 4c*, the long period of which is $D \approx 31$ nm. This reflection can be associated with an alternating parallel arrangement of large HB lamellar crystals and HI amorphous layers, in consideration of the fact that crystallization is the driving force of phase separation in the solution. Thus the crystal thickness $e \approx 8$ nm is determined from the relation

$$e = \phi_{HB}D \quad (5)$$

which assumes that the lateral extent of the lamellar crystals is very large compared with their thickness.

Figure 5 displays a schematic view of the mesomorphic structure of the two forms of the HBIB block polymer crystallized from the melt and from solution. In the melt-crystallized sample, the segregated HB blocks are liable to adopt a switchboard-like crystalline topology which involves good molecular cohesion within the microdomains (*Figure 5a*). On the other hand, owing to the dilution effect, the HB blocks of the solution-crystallized sample are capable of building up single crystal like microdomains with predominant regular chain folding (*Figure 5b*). These radically different chain topologies are expected to give rise to specific mechanical properties for the two forms of the HBIB block polymer.

Tensile drawing

The first stress–strain cycle and subsequent extension up to failure of a melt-crystallized HBIB sample are shown in *Figure 6*. The material behaves as a crosslinked elastomer, with a filler effect due to the ductile HB phase which ensures a physical crosslinking of the chains. Indeed, the intermolecular crystallization of the HB blocks (*Figure 5a*) provides strength and stiffness to the crosslinking microdomains. The hysteresis of the first stress–strain cycle which reveals plastic deformation processes in the semi-crystalline HB phase contains a viscoelastic contribution, as indicated by the partial recovery of the material on the second extension. The stress levelling which occurs for $7 < \alpha < 10$ results from the fibrillation of the HB microdomains before failure, as will be shown in the following structural study of the deformation.

On the other hand, the drawing behaviour of the

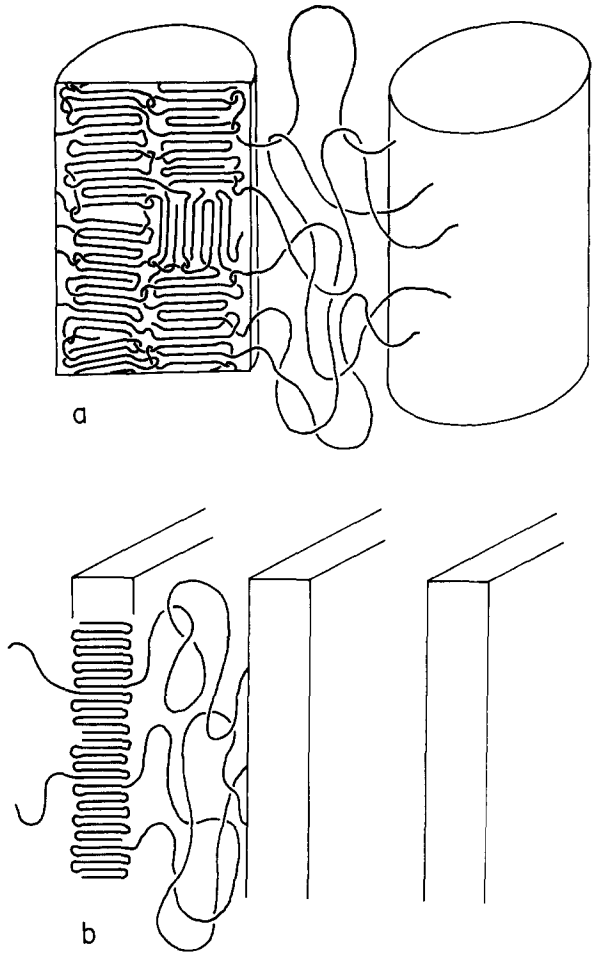

Figure 5 Molecular models for (a) the melt-crystallized form and (b) the solution-crystallized form of the HBIB triblock polymer

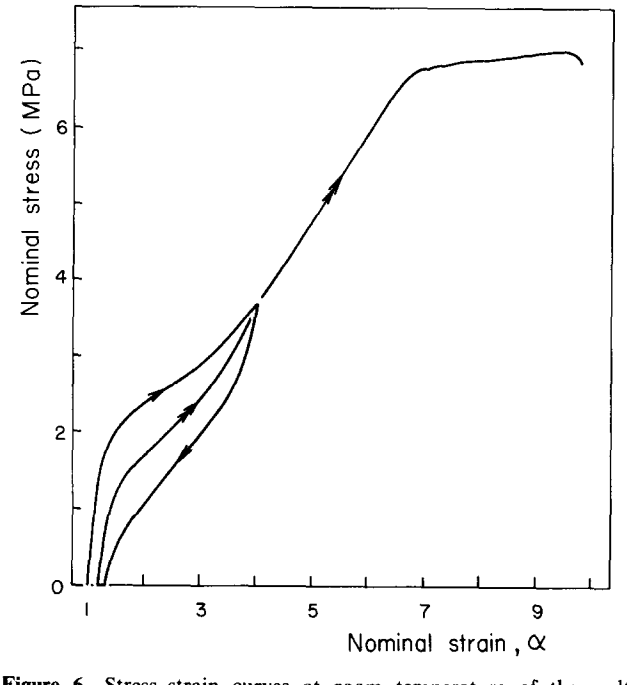

Figure 6 Stress–strain curves at room temperature of the melt-crystallized HBIB: →←, first cycle; →→←, second extension

solution-crystallized HBIB shown in *Figure 7a* is characterized by a drawing plateau at a low stress $\sigma \approx 1$ MPa and a very high extension at rupture $\alpha = 24$. The material looks like a very low crystallinity homopolyethylene which flows under stress[29]. The creep of the HBIB block polymer crystallized from solution indicates a very poor crosslinking effect of the chains. This mechanical weakness relies on the very structure of the HB microdomains grown from solution (*Figure 5b*). Indeed, chain-folded single crystals of homopolymers crystallized from dilute solution are well known to be very brittle[24,30–32]. However, the fragments from broken single crystals are bound together by thin fibrils having very high draw ratios. The fibrils grow by unfolding of the regularly folded chains from the fracture surfaces. Ethylene/propylene[32] and ethylene/butene[33] random copolymers crystallized from dilute solutions have notably been reported to exhibit draw ratios at rupture close to $\alpha = 50$. These results provide an explanation for both the low strength and the unusually high drawing of the solution crystallized HBIB. The structural aspects will be discussed further.

It is noteworthy that after being melted and recrystallized by slow cooling, the originally solution-crystallized HBIB displays a tensile drawing behaviour close to the directly melt-crystallized HBIB (compare *Figure 7b* and *Figure 6*). This is evidence of a healing phenomenon in the metastable HB phase due to coalescence and re-entangling of the molten blocks which involves restoration of the physical crosslinking effect in a more stable mesomorphic structure.

Viscoelastic properties

The variations with temperature of the storage modulus, E', and loss factor, $\tan \delta$, of the melt-crystallized

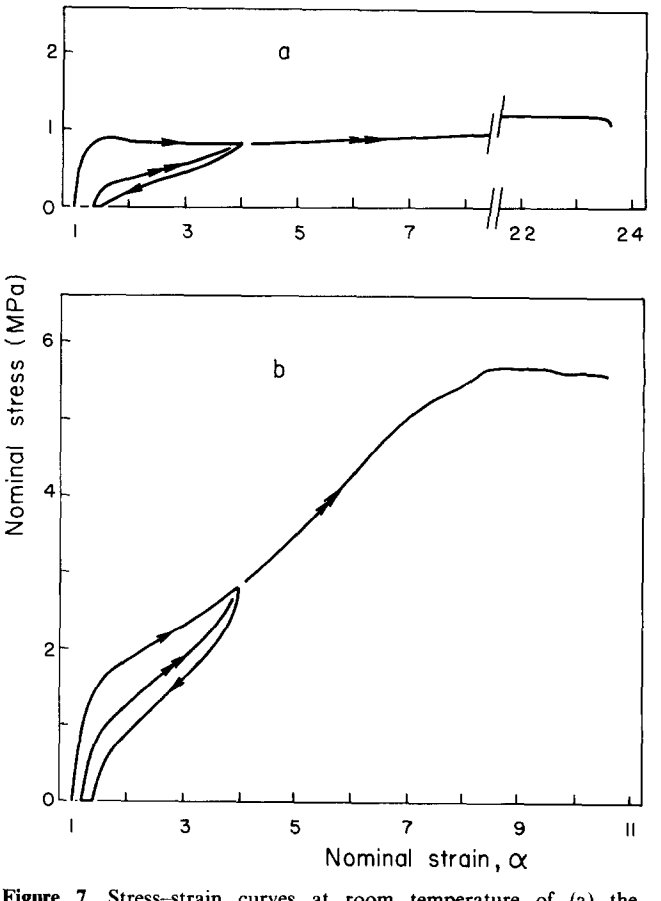

Figure 7 Stress–strain curves at room temperature of (a) the solution-crystallized HBIB and (b) the same material recrystallized after melting: →←, first cycle; →→←, second extension

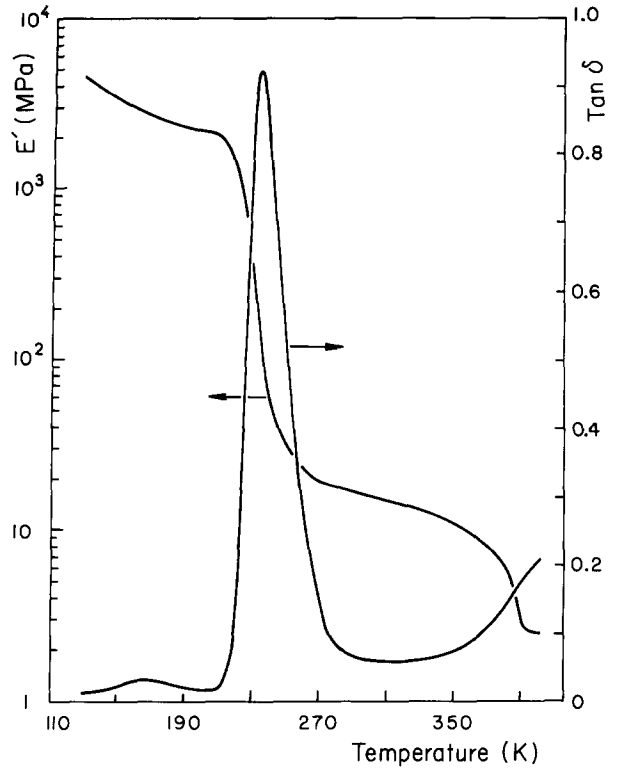

Figure 8 Dynamic storage modulus, E', and loss factor, tan δ, of the melt-crystallized HBIB as a function of temperature

HBIB are shown in *Figure 8*. The glass transition of the HI phase gives rise to a sharp absorption peak in the tan δ curve associated with a large drop in E' in the temperature range 210–270 K. On the other hand, the slow decay of E' and the steady increase of tan δ in the range 350–390 K are relevant to the α mechanical relaxation and gradual melting of the HB phase. Between the two transitions where the material behaves like a physically crosslinked elastomer, the storage modulus $E' \approx 15$ MPa is significantly greater than that of pure vulcanized rubber, i.e. about 1 MPa[34]. This results from the filler effect of the hard crosslinking HB phase, as previously suggested from the hysteresis of the first stress–strain cycle (*Figure 6*).

The viscoelastic behaviour of the HBIB block polymer in its solution-crystallized form is largely different from that of the melt-crystallized form in the temperature range of the HB phase relaxation, as can be judged from *Figure 9*. The storage modulus exhibits around $T = 380$ K an unusual maximum indicative of a structural metamorphosis which induces a mechanical improvement of the material before its final collapse due to complete melting of the HB phase. This is perfectly consistent with the coalescence of the HB blocks from a metastable morphology into a stable one, as discussed in the preceding section. It is particularly relevant to the incompatibility between the HB and HI blocks in the molten state since an eventual miscibility would have resulted in a steady drop of the storage modulus in the melting temperature range of the HB phase. This result supports our previous conclusion of HB and HI incompatibility from thermal data as well as thermodynamic considerations.

It deserves mention that, in contrast to the melt-crystallized HBIB (*Figure 8*), the solution-crystallized HBIB shows a clear α-relaxation maximum in the tan δ curve, around $T = 350$ K (*Figure 9*). This is not really surprising since it has been reported, for homopolyethylene, that solution-crystallized samples display a much more pronounced α-relaxation peak in the tan δ curve than melt-crystallized samples[35].

Structural changes upon deformation

The structural analysis of the room temperature deformation has been investigated via combined SAXS and WAXS measurements as a function of draw ratio. *Figure 10* shows SAXS and WAXS patterns of melt-crystallized HBIB samples. The two first rows of *Figure 10a* refer to the interdomain and intercrystallite scattering, respectively, while the third row shows schematic diagrams of both diffractions. The WAXS patterns of *Figure 10b* display the (110) and (200) reflections characteristic of the polyethylene-like lattice in the HB crystalline phase together with the inner diffuse halo due to the rubbery HI matrix and the amorphous part of the HB phase. The first sharp SAXS ring transforms gradually into a diagonal reflection, which indicates an orientation process of the HB microdomains toward a preferred direction. We have reported a similar phenomenon for the deformation of a hydrogenated SBS triblock polymer[36] with a mesomorphic structure consisting of PS cylinders embedded in a rubbery matrix. The strain-induced orientation of the PS cylinders inclined with respect to the draw axis was ascribed to a homogeneous shear of the grains (regions of well organized structure) according to the lowest energy path of deformation. However, contrary to the glassy PS cylinders, the ductile semi-crystalline HB microdomains in the melt-crystallized HBIB are prone to undergo a fibrillar transformation whose process has been largely described by Peterlin[37]. This is expected to bring the

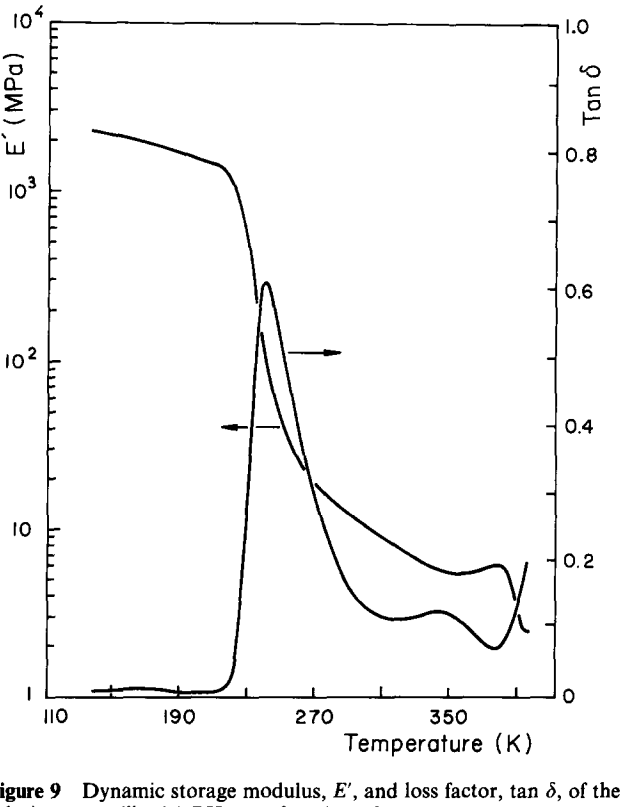

Figure 9 Dynamic storage modulus, E', and loss factor, tan δ, of the solution-crystallized HBIB as a function of temperature

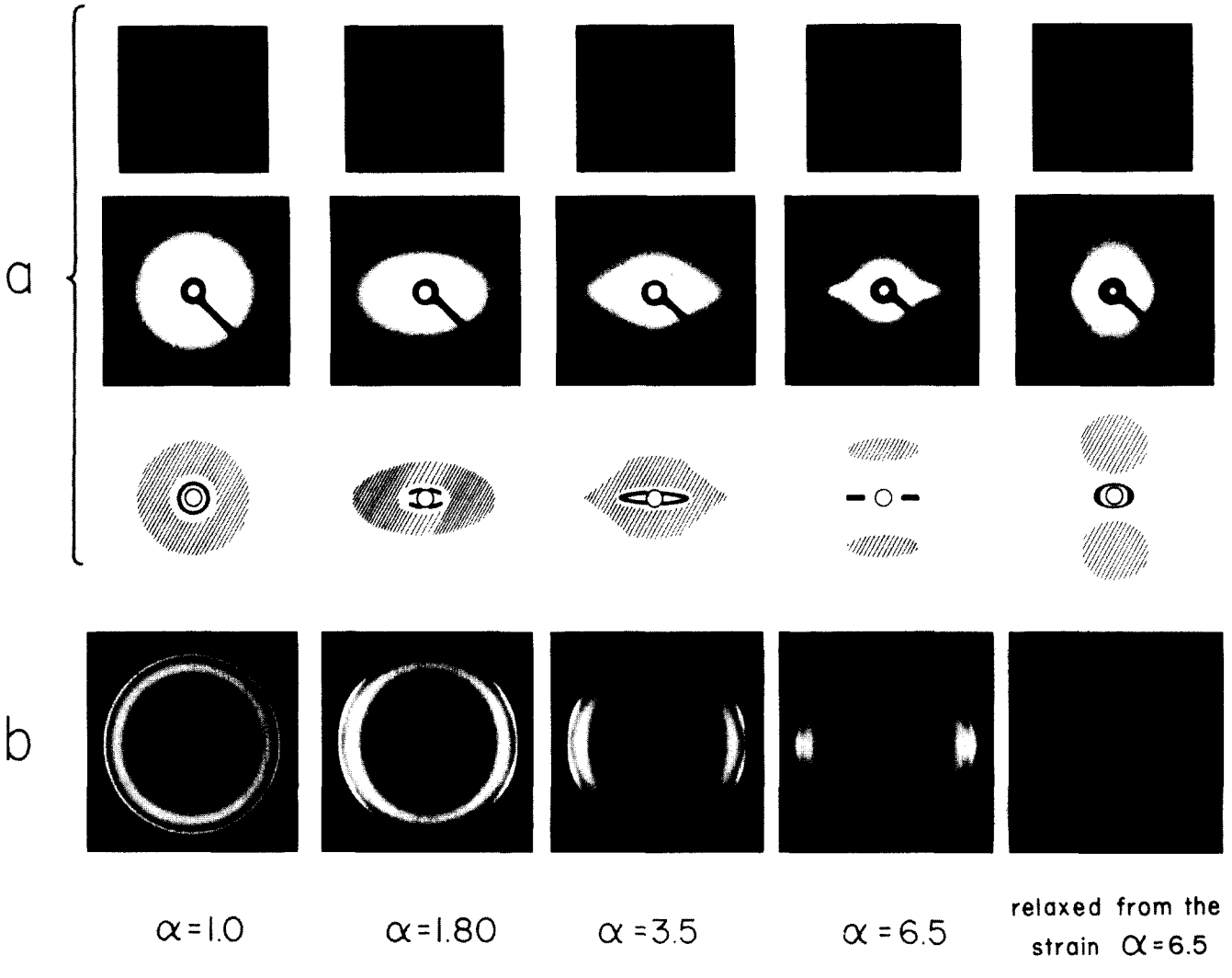

Figure 10 Evolution with draw ratio, α, of (a) SAXS and (b) WAXS patterns of the melt-crystallized HBIB deformed at room temperature. The draw direction is vertical

highly drawn crosslinking microdomains parallel to the tensile axis as indicated by the change of the first SAXS reflection into equatorial spots for $\alpha = 6.5$ (*Figure 10a*). The fibrillar transformation of the HB microdomains also is corroborated by the build up of meridional reflections associated with the intercrystalline scattering (see *Figure 10a* for $\alpha = 6.5$) together with the *c*-axis orientation of the unit cell as revealed by the equatorial position of both (110) and (200) crystalline reflections (see *Figure 10b* for $\alpha = 6.5$).

Note that, for the strain $\alpha = 6.5$, the rubbery HI matrix is highly oriented, as shown by the strong equatorial reinforcement of the inner amorphous halo in the WAXS pattern of *Figure 10b*. After unloading of the sample, the nearly uniform intensity of the amorphous WAXS halo gives evidence of the recovery of the HI matrix close to its isotropic state, while the HB microdomains keep their fibrous structure.

SAXS and WAXS patterns concerned with the solution-crystallized HBIB are reported in *Figure 11*. The unique broad SAXS ring of *Figure 11a* turns into diagonal reflections which evolve toward the equator as the draw ratio increases. This is clearly indicative of a gradual orientation of the large lamellar HB crystals parallel to the draw direction. On the other hand, the nearly uniform intensity of the amorphous halo in the WAXS patterns of *Figure 11b* reveals a very poor orientation of the chains of the rubbery HI matrix, notably for $\alpha = 6.5$, in opposition to the strong amorphous chain orientation in the melt crystallized sample. This result absolutely corroborates the creep effect in the solution-crystallized HBIB previously concluded from the tensile drawing study (i.e. high deformation under low stress accompanied by low amorphous chain orientation).

In parallel, the WAXS patterns of *Figure 11b* show a diagonal reinforcement of the (200) reflection, while the (110) reflection concentrates on the equator along with increasing deformation. These features are relevant to a *b*-axis orientation parallel to the draw direction. Such an orientation is quite unusual for plastic deformation at large strains, the main consequence of the plastic flow being the orientation of the *c*-axis (molecular chain axis) in the draw direction.

The explanation for the *b*-axis orientation in the solution-crystallized HBIB may lie in the fact that low density polyethylene[30,38], as well as ethylene copolymers[39], gives rise to laurel-leaf-like single crystals with the *b*-axis aligned parallel to the major axis. Besides, block polymers containing a crystallizable species are well known to display the same crystal habits as their respective parent homopolymers when crystallized from dilute solution[10–12]. *Figure 12* shows schematically the

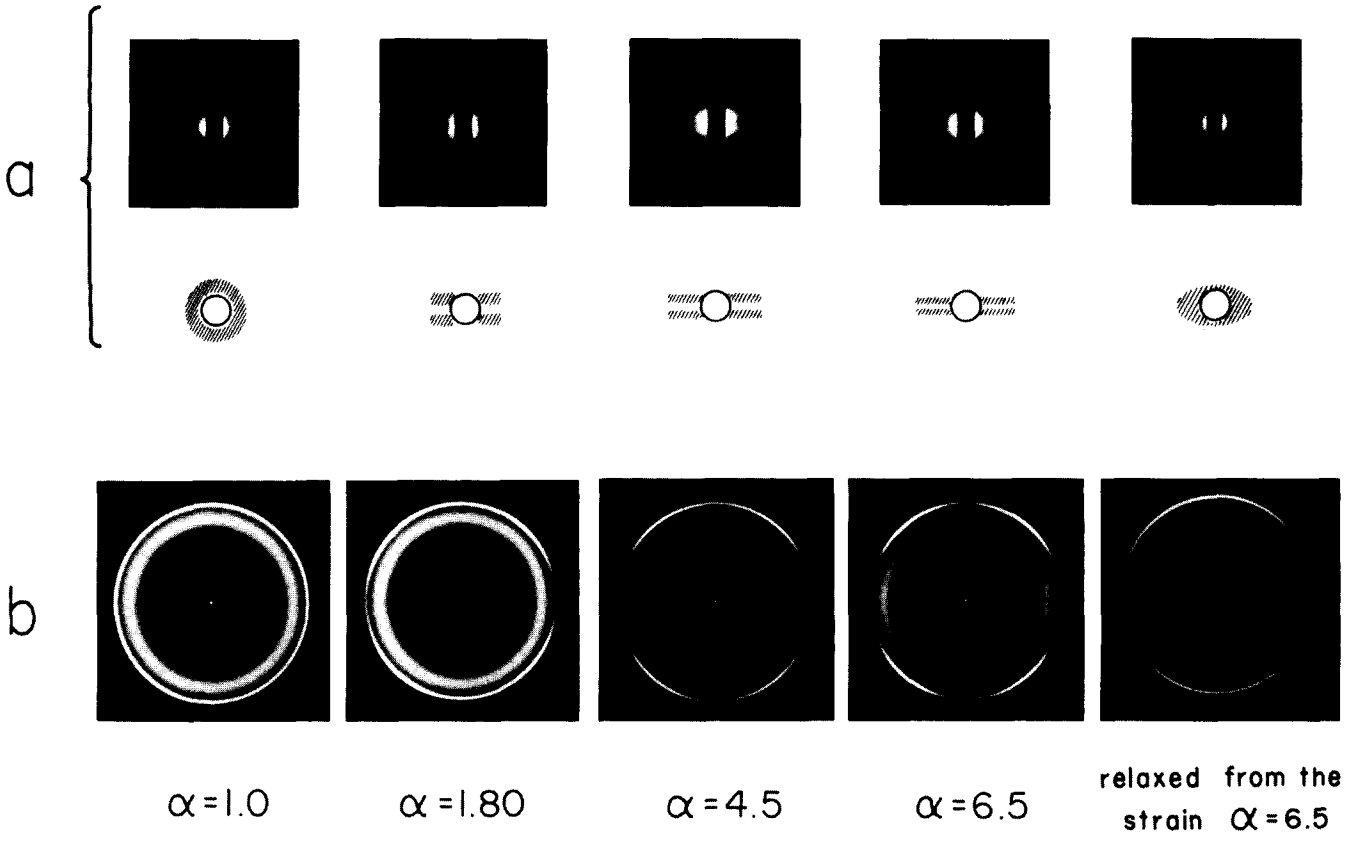

Figure 11 Evolution with draw ratio, α, of the (a) SAXS and (b) WAXS patterns of the solution-crystallized HBIB deformed at room temperature. The draw direction is vertical

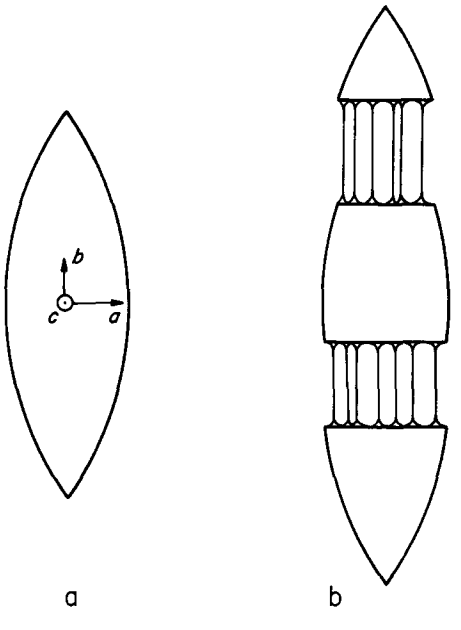

Figure 12 Schematic model for the structure of HB single crystals in the solution crystallized HBIB: (a) as grown from solution; (b) after drawing. The draw direction is vertical

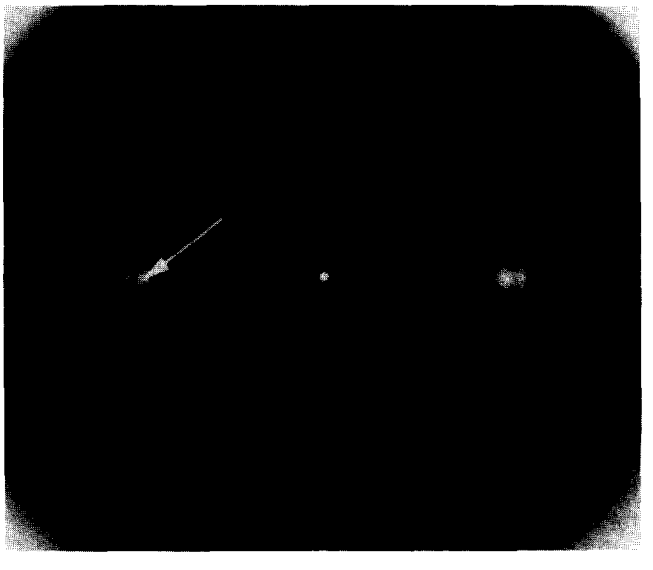

Figure 13 WAXS pattern of a solution-crystallized HBIB sample drawn at $\alpha=20$. The arrow indicates the (010) monoclinic reflection. The draw direction is vertical

most probable shape of the HB crystals in the solution-crystallized HBIB. Accordingly, the *b*-axis orientation under tensile drawing appears as a logical effect of the orientation of the crystals themselves. However, borrowing from the general behaviour of homopolymer single crystals under strain[24,30–32], we can expect the HB crystals to be very fracture prone with a propensity to develop microfibrils by chains unfolding from the fracture surfaces, according to the sketch of *Figure 12b*. In this connection, it is worth examining the WAXS pattern of a solution-crystallized HBIB sample drawn up to $\alpha=20$, which is reported in *Figure 13*. Both *b*-axis and *c*-axis orientations are observed on this figure, in agreement with the scheme of *Figure 12b*, which implies coexistence of single crystal fragments and chain unfolded microfibrils having, respectively, the very orientation mentioned above. The clear presence of an additional equatorial spot characteristic of the (010) reflection of monoclinic polyethylene (*Figure 13*) suggests the build up of internal stresses within the microfibrils[40–42].

Although speculative, the model of *Figure 12* has the merit of shedding light on the mechanical properties of the solution-crystallized HBIB, namely the strong creep effect and very large extension at break already discussed in the tensile drawing section, besides its consistency with the structural analysis of the deformation.

CONCLUSION

Melt crystallization is a necessary condition to impart good elastomeric properties to the HBIB triblock polymer. This relies on the fact that liquid–liquid phase separation of the unlike species in the melt is required to allow bulk crystallization of the HB blocks within microdomains which act as physical crosslink points. The chains of the rubbery HI matrix show a strong orientation under extension and the HB microdomains undergo a plastic deformation similar to the fibrillar transformation in polyethylene before rupture. Solution crystallization generates brittle single crystals which are not able to play a crosslinking function. The HI chains exhibit a very low orientation up to the rupture which occurs at a draw ratio of 22. This is clearly relevant to creep under stress of the rubbery matrix. The unusual *b*-axis orientation of the crystalline HB phase can be ascribed to the orientation of the prolate single crystals parallel to the draw direction. The microfibrils which develop from the fracture surfaces of the broken single crystals are responsible for the very high extension at break and allow conservation of the *b*-axis orientation of the crystalline fragments.

The influence of the morphogenesis, namely the crystallization conditions, on the mechanical properties of triblock polymers of the HBIB type can *a priori* be extended to all thermoplastic elastomers having semi-crystalline stiff blocks since the structural basis of the interpretation proposed in the present paper is not specific to polyethylene-based systems. It is worth mentioning that TCB–I–TCB triblock polymers studied by Kuo and McIntyre support this statement very well.

ACKNOWLEDGEMENTS

This work was supported by the National Sciences and Engineering Research Council of Canada and the Quebec Ministry of Education.

REFERENCES

1 Noshay, A., and McGrath, J. E. 'Block Copolymers; Overview and Critical Survey', Academic Press, New York, 1977
2 Ambrose, R. J. and Aggarwal, S. L. (Eds) 'Advances in Preparation and Characterization of Multiphase Polymer Systems', *J. Polym. Sci., Polym. Symp.* 1977, **60**
3 Gallot, B. *Adv. Polym. Sci.* 1978, **29**,85
4 Bostick, E. E. in 'Block Copolymers', (Ed. S. L. Aggarwal), Plenum Press, New York, 1970, p. 237
5 Morton, M. and Mikesell, S. L. *J. Macromol. Sci. Chem.* 1973, **A7**, 1391
6 Hale, P. T. and Pope, G. A. *Eur. Polym. J.* 1975, **11**, 677
7 Lenz, R. W., Dror, M., Jorgensen, R. and Marchessault, R. H. *Polym. Eng. Sci.* 1978, **18**, 937
8 Foss, R. P., Jacobson, H. W., Cripps, H. N. and Sharkey, W. H. *Macromolecules* 1979, **12**, 1210
9 Petit, D., Jérome, R. and Teyssié, P. *J. Polym. Sci., Polym. Chem. Edn.* 1979, **17**, 2903
10 Lotz, B., Kovacs, A. J., Basset, G. A. and Keller, A. *Kolloid Z. Z. Polym.* 1966, **209**, 115
11 Savelief, M., Lotz, B. and Kovacs, A. J. *Inf. Chim.* 1973, **118**, 199
12 Hirata, E., Ijitsu, T., Soen, T., Hashimoto, T. and Kawai, H. *Polymer* 1975, **16**, 249
13 Kuo, C. and McIntyre, D. J. *J. Polym. Sci., Polym. Phys. Edn.* 1975, **13**, 1543
14 Robitaille, C. and Prud'homme, J. *Macromolecules* 1983, **16**, 665
15 Morris, H. L. in 'Handbook of Thermoplastic Elastomers', (Ed. B. M. Walker) Van Nostrand–Reinhold, New York, Ch. 2, 1979
16 Falk, J. C. and Schlott, R. J. *Macromolecules* 1971, **4**, 152
17 Cowie, J. M. G. and McEwen, I. J. *Macromolecules* 1977, **10**, 1124
18 Laramée, A., Goursot, P. and Prud'homme, J. *Makromol. Chem.* 1975, **176**, 3029
19 Falk, J. C. and Schlott, R. J. *Angew. Makromol. Chem.* 1972, **21**, 17
20 Mohajer, Y., Wilkes, G. L., Wang, I. C. and McGrath, J. E. *Polymer* 1982, **23**, 1523
21 Mohajer, Y., Wilkes, G. L., Wang, I. C. and McGrath, J. E. *Am. Chem. Soc. Symp. Ser.* 1982, **193**, 119
22 Prud'homme, J., Roovers, J. E. L. and Bywater, S. *Eur. Polym. J.* 1972, **8**, 901
23 Bronstert, K., Ladenberger, B. and Fahrbach, G. Badische Anilin – und Soda – Fabrik A.-G., Ger. offen. 2 013 263, 1971; US Patent 3 673 281, 1972
24 Wunderlich, B. 'Macromolecular Physics', Vol. 1, 'Crystal Structure, Morphology and Defects', Academic Press, New York, 1973, Ch. 4
25 *Faraday Discuss. Chem. Soc.* 1979, **68**
26 Brandrup, J. and Immergut, E. H. (Eds.) 'Polymer Handbook', 2nd edn., Wiley–Interscience, New York, 1975, Ch. IV, pp. 337–9
27 Lindsay, G. A., Singleton, C. J., Carman, C. J. and Smith, R. W. *Adv. Chem. Ser.* 1979, **176**, 367
28 Morèse-Séguéla, B., St-Jacques, M., Renaud, J.-M. and Prud'homme, J. *Macromolecules* 1980, **13**, 100
29 Sperati, C. A., Franta, W. A. and Starkweather Jr., H. W. *J. Am. Chem. Soc.* 1953, **75**, 6127
30 Geil, P. H. 'Polymer Single Crystals', Wiley–Interscience, New York, 1963, Ch. II and VII
31 Gleiter, H. and Petermann, J. *J. Polym. Sci., Polym. Lett. Edn.* 1972, **10**, 877
32 Holdworth, P. J. and Keller, A. *J. Polym. Phys.* 1968, **6**, 707
33 Domszy, R. C., Alamo, R., Mathieu, P. J. M. and Mandelkern, L. *J. Polym. Sci., Polym. Phys. Edn.* 1984, **22**, 1727
34 Treloar, L. R. G. 'The Physics of Rubber Elasticity', 2nd edn., Oxford University Press, London, 1968, Ch. XIV
35 Ward, I. M. 'Mechanical Properties of Solid Polymers', 2nd edn., Wiley–Interscience, New York, 1983, Ch. 8
36 Seguela, R. and Prud'homme, J. *Macromolecules* 1988, **21**, 635
37 Peterlin, A. *Colloid Polym. Sci.* 1975, **253**, 809
38 Rybnikar, F. *J. Macromol. Sci. Phys.* 1975, **B11**, 329
39 Holdsworth, P. J. and Keller, A. *J. Polym. Sci., Polym. Lett. Edn.* 1967, **5**, 605
40 Frank, F. C., Keller, A. and O'Connor, A. *Phil. Mag.* Ser. 8, 1958, **3**, 64
41 Kiho, H., Peterlin, A. and Geil, P. H. *J. Appl. Phys.* 1964, **35**, 1599
42 Alan, P. and Bevis, M. *Proc. R. Soc. Lond.* 1974, **341**, 75